Contribution of the nuclear field shift to kinetic uranium isotope fractionation

A.R. Brown, Y. Roebbert, A. Sato, M. Hada, M. Abe, S. Weyer, R. Bernier-Latmani

Supplementary Information

The Supplementary Information includes:

Experimental Section

Preparation of the U multi-isotope standard

The ^{233}U, ^{235}U, ^{236}U, ^{238}U standard was prepared by mixing the reference materials IRMM-184 (natural U) and IRMM-3636 (a 1:1 mix of the ^{233}U and ^{236}U 'double spike') at an approximate ratio of 25:1 to give a $^{236/233}$U/^{235}U ratio of ~3. The nitric acid matrix was then evaporated and replaced with 6 N ultra-pure HCl, followed by evaporation and replacement with 0.1 N ultra-pure HCl. The standard was then moved to an anoxic chamber (100 % N_2, <0.1 ppm O_2; MBraun, Germany).

Culturing of *Shewanella oneidensis*

Shewanella oneidensis MR-1 was grown in oxic Luria-Bertani (LB) medium to mid-late exponential phase. Cultures were then harvested by centrifugation for 10 min at 5000 × *g* and washed three times in a sterile anoxic buffer containing 30 mM sodium bicarbonate and 20 mM piperazine-N,N′-bis(2-ethanesulfonic acid) (PIPES) at pH 7.3. Finally, the cultures were resuspended in the same medium to an appropriate density, prior to addition to experimental reactors.

Reduction of U^{VI} by *S. oneidensis*

Anoxic reactors containing 30 mM sodium bicarbonate and 20 mM PIPES at pH 7.3 were prepared. 20 mM sodium lactate was supplied as the electron donor. All experimental media were autoclaved, flushed with pure and sterile N_2 for several hours and then stored in the dark at ~25 °C inside an anoxic chamber. 200 μM of the U^{VI} multi-isotope standard was added from an anoxic ~20 mM U chloride stock. Aliquots of the anoxic *S. oneidensis* cell suspensions were then

added to the reactors to give a final optical density of 1, as measured at 600 nm (OD_{600nm}) using a UV-vis spectrophotometer, which was equivalent to approximately 5×10^8 cells mL^{-1}. Periodically, samples were removed for the analysis of aqueous U^{VI} concentrations and isotope ratio analysis. Approximately 0.5 mL was removed using a sterile, anoxic syringe and needle, and the sample was filtered through a 0.22 μm PTFE filter. This process removes both the solid phase U^{IV} and bacterial cells and thus, prevents any further reduction. Samples were then stored at −20 °C.

U isotope ratio analysis

Samples were first weighed and evaporated to dryness. The samples were treated with a mixture of 200 μl 14 M HNO$_3$ and 200 μl H$_2$O$_2$ (30 %) to destroy organic materials. Uranium was then purified by ion-exchange chromatography according to a method described by Weyer *et al.* (2008). The samples were dissolved in 1 mL 3 M HNO$_3$ and U was purified on Eichrom UTEVA resin.

U isotope measurements were performed at Leibniz Universität Hannover with a Thermo-Finnigan Neptune multi-collector ICP-MS (MC-ICP-MS), similar to the protocol published by Noordman *et al.* (2015). For sample introduction, a Cetac Aridus-II desolvation system equipped with a perfluoroalkoxy alkane (PFA) nebuliser with a sampling rate of 100 μL/min was used to enhance sensitivity and to reduce solvent-based interferences such as oxides and hydrides. Additionally, a standard Ni sampling cone and a Ni X skimmer cone were used in combination with a 0.8 mm copper ring (spacer). With this setup, a 210 ng/g solution achieved a signal of between 130 and 200 V on ^{238}U in low mass resolution mode.

The abundance sensitivity was determined before each analysis term and was typically ≤0.1 ppm of the ^{238}U signal at mass 236 (determined on a spike-free solution), resulting in negligible tail correction.

All samples and standards were measured with 320 s total integration time (80 cycles at 4 s integration time). A standard sample bracketing method was applied during analysis, *i.e.* one sample measurement was bracketed by two standard measurements. The results for all sample analyses are presented in the delta notation with respect to ^{235}U and relative to the U standard, *e.g.*, for ^{238}U:

$$\delta^{238}U \ [\text{‰}] = \left[\frac{(^{238}U/^{235}U)_{sample}}{(^{238}U/^{235}U)_{standard}} - 1 \right] \cdot 1000. \qquad \text{(Eq. S-1)}$$

Each sample was analysed three times and the precision is given as two standard deviations (2 s.d.) of the replicate analysis for each sample (with an average error of 0.19 ‰ for δ^{238}U). Additionally, reproducibility and accuracy was determined by replicate analyses of the U-standards IRMM-184 (−1.17 ‰ ± 0.05) and REIMEP 18-A (−0.28 ‰ ± 0.07) relative to CRM-112A during each analysis session and the results agreed with those previously reported in the literature, within uncertainties (Weyer *et al.*, 2008; Richter *et al.*, 2010; Brennecka *et al.*, 2011; Noordmann *et al.*, 2015; Li and Tissot, 2023).

Rayleigh distillation models

Isotope fractionation factors were determined by fitting Rayleigh distillation models to the measured isotopic signatures, according to the method described in Scott *et al.* (2004) and using the following formula:

$$\delta_t = (\delta_0 + 1000 \ \text{‰}) \left[\frac{c_t}{c_0} \right]^{\alpha - 1} - 1000 \ \text{‰}, \qquad \text{(Eq. S-2)}$$

where c_0 and δ_0 are the initial concentration and isotopic composition of U^{VI}, and c_t and δ_t are the concentration and isotopic composition of U^{VI} at time t. The fractionation factors (ε) were obtained from the slope ($\alpha - 1$) of the linear regression of the experimental data in linearised plots of ln(δ^{238}U + 1000 ‰) *versus* ln(c_t/c_0), where $\varepsilon = (\alpha - 1) \times 1000$.

Decomposition of ε

To calculate the contribution of the nuclear field shift effect (NFSE) and the mass effect to the fractionation factors obtained for each isotope during the enzymatic reduction, we used the methods of Fujii *et al.* (2009) and Moynier *et al.* (2009) to obtain the scaling factors of the conventional mass effect and the nuclear field shift term that appear in Bigeleisen's (1996) equation:

$$\ln \alpha = \left(\frac{hc}{kT}\right) f_s \times A + \frac{1}{24}\left(\frac{\hbar}{kT}\right)^2 \frac{\delta m}{mm'} \times B, \qquad \text{(Eq. S-3)}$$

where f_s is the field shift frequency, h is the Planck constant, c is the speed of light in a vacuum, k is the Boltzmann constant, T is temperature and $\hbar$ is the reduced Planck constant; m and m' are the masses of the heavy and light isotopes and δm equates to the mass difference, $m - m'$. Here, A is the scaling factor for the nuclear field shift effect (the first term on the right-hand side of Eq. S-3) and B is the scaling factor of the mass-dependent vibrational effect. We modified the mass-dependent fractionation term for the kinetic effect according to Zheng and Hintelmann (2010) after Young *et al.* (2002). As the field shift frequency is proportional to the mean-squared nuclear charge radius ($\delta\langle r^2 \rangle_{235,i} = \delta\langle r^2 \rangle_i - \delta\langle r^2 \rangle_{235}$) (Bigeleisen, 1996), at constant temperature, Equation S-3 can be simplified to:

$$\ln \alpha = \delta\langle r^2 \rangle \times a + \ln\left(\frac{m_{235}}{m_i}\right) \times b, \qquad \text{(Eq. S-4)}$$

where a and b are new scaling factors. Equation S-4 can then be linearised by rearrangement to give:

$$\frac{\varepsilon_i}{\ln(m_{235}/m_i)} = \frac{\delta\langle r^2 \rangle_{235,i}}{\ln(m_{235}/m_i)} \times a + b. \qquad \text{(Eq. S-5)}$$

The scaling factors were then obtained from linear plots of the above parameters. The fractionation factors, ε ($\approx \ln \alpha$), for each isotope of mass m_i, with respect to ^{235}U (m_{235}), were obtained from the Rayleigh distillation models. Mean square nuclear charge radii ($\delta\langle r^2 \rangle_{235,i} = \delta\langle r^2 \rangle_i - \delta\langle r^2 \rangle_{235}$) for each atomic mass were taken from Angeli and Marinova (2013). The contributions of the nuclear field shift term and the mass term to the overall observed fractionation factor were then calculated using Equation S-4.

Ab initio calculation of ε^{eq} between U^{VI} and U^{IV}

We modelled the tri- and di-carbonate complexes, *i.e.* UO$_2$(CO$_3$)$_3^{4-}$ and UO$_2$(CO$_3$)$_2^{2-}$, as the U^{VI} species because they are the dominant U^{VI} species under our experimental conditions (Fig. S1). The dominant product of U^{VI} reduction by *S. oneidensis* MR-1 under these same conditions is a non-uraninite U^{IV} (Stylo *et al.*, 2015). As ningyoite (CaU(PO$_4$)$_2$) is a close analogue of these non-crystalline biotic reduction products (Bernier-Latmani *et al.*, 2010; Alessi *et al.*, 2014; Sato *et al.*, 2021), we modelled the U^{IV} as a cluster of ningyoite (H$_{26}$CaU(PO$_4$)$_{10}^{2+}$), as established previously (Sato *et al.*, 2021).

ε^{eq} was calculated as the sum of the nuclear mass term, $\ln K_{nm}$ (Bigeleisen and Mayer, 1947), and the NFSE term, $\ln K_{fs}$ (Bigeleisen, 1996; Nomura *et al.*, 1996; Fujii *et al.*, 2009), at a temperature of 298 K, the same as the microbial U^{VI} reduction experiments:

$$\varepsilon^{eq} = \ln K_{nm} + \ln K_{fs}. \qquad \text{(Eq. S-6)}$$

The nuclear mass term, $\ln K_{nm}$, was calculated as a difference in the logarithms of the reduced partition function ratio, β, of U^{IV} and U^{VI}:

$$\ln K_{\mathrm{nm}} = \ln \beta\left(U^{\mathrm{IV}}\right) - \ln \beta\left(U^{\mathrm{VI}}\right) \qquad , \qquad \text{(Eq. S-7)}$$

where, $\ln \beta$ is described by the harmonic frequencies, ν:

$$\ln \beta = \ln\left[\prod_i \frac{u_i}{u_i'} \frac{e^{-u_i/2}/(1-e^{-u_i})}{e^{-u_i'/2}/\left(1-e^{-u_i'}\right)}\right], \quad u_i \equiv \frac{h\nu_i}{k_{\mathrm{B}}T}. \qquad \text{(Eq. S-8)}$$

Here, h is the Planck constant, k_{B} is the Boltzmann constant and T is the absolute temperature. The indices of the vibrational modes are denoted by the subscript i, and the quantities for the light isotope are indicated by the prime notation.

The NFSE term, $\ln K_{\mathrm{fs}}$, was calculated from the ground-state electronic energies of isotopologues of U^{VI} and U^{IV}:

$$\ln K_{\mathrm{fs}} = \left[\left\{E\left(^{238}U^{\mathrm{VI}}\right) - E\left(^{235}U^{\mathrm{VI}}\right)\right\} - \left\{E\left(^{238}U^{\mathrm{IV}}\right) - E\left(^{235}U^{\mathrm{IV}}\right)\right\}\right]/k_{\mathrm{B}}T \qquad . \qquad \text{(Eq. S-9)}$$

The geometry optimisation and the vibrational analysis for the calculation of $\ln K_{\mathrm{nm}}$ were conducted with the Gaussian 09 software package (Frisch *et al.*, 2009). These calculations used density functional theory (DFT) with the hybrid exchange-correlation functional consisting of Becke's (1993) three-parameter non-local hybrid exchange potential with Lee-Yang-Parr non-local functionals (B3LYP) (Lee *et al.*, 1988; Stephens *et al.*, 1994). We used Stuttgart-type small core relativistic pseudopotentials named ECP60MWB (Küchle *et al.*, 1994) with a contracted Gaussian basis set of [10s, 9p, 5d, 5f, 3g] (Cao and Dolg, 2004) for U and the 6-31+G(d) basis set for the remaining atoms. The solvation effects were modelled by using the polarisable continuum model (Scalmani and Frisch, 2010) assuming the water solvent condition, *i.e.* a dielectric constant of 78.39.

Vibrational frequencies for the ^{233}U isotopologue could not be calculated because the mass data for ^{233}U is not supported in Gaussian 09. Therefore, $\ln \beta$ for ^{233}U/^{235}U was estimated by extrapolating the data from $\ln \beta$ for ^{234}U/^{235}U, ^{236}U/^{235}U, and ^{238}U/^{235}U using the proportional relationship between $\ln \beta$ and mass.

For the optimised ground-state geometry, we performed the electronic energy calculations with DIRAC16 software package (Jensen *et al.*, 2016; Saue *et al.*, 2020) at the Hartree-Fock (HF) and DFT levels with the exact two-component (X2C) relativistic Hamiltonian (Iliaš and Saue, 2007; Liu, 2010; Saue, 2011; Knecht *et al.*, 2022) to calculate $\ln K_{\mathrm{fs}}$. In the X2C-DFT calculations, we used the B3LYP hybrid exchange-correlation functional (Lee *et al.*, 1988; Becke, 1993; Stephens *et al.*, 1994). We used the Dyall.cv2z basis set (Dyall, 2007) for U and the 6-31+G(d) basis set for the remaining atoms.

To model the nuclear volume of each isotope, we used the Gaussian-type finite nucleus model (Visscher and Dyall, 1997) with the experimentally determined root-mean-square nuclear charge radii of ^{233}U, ^{235}U, ^{236}U, and ^{238}U which are 5.8203 fm, 5.8337 fm, 5.8431 fm, and 5.8571 fm, respectively (Angeli and Marinova, 2013).

For each molecular model, we optimised only the wave functions of ^{238}U isotopologue and used them to calculate the electronic energies of other isotopologues. This strategy is based on the demonstration of the previous studies that the effect of the optimisation for a single isotope is minor (Fricke and Waber, 1972; Filatov, 2007; Knecht *et al.*, 2011) and may suppress the unphysical numerical errors caused by the optimisation of the wave functions of all the isotopologues (Sato *et al.*, 2021).

Supplementary Table

Table S-1   ln K_{fs} (nuclear field shift effect term), ln K_{nm} (nuclear mass term) and ε^{eq} (total fractionation factor) for the reduction of the two dominant species of U^{VI}-carbonate to U^{IV}. ln K_{fs} was calculated by either X2C-Hartree-Fock (X2C-HF) or X2C-B3LYP, and the values are shown in the columns of "HF" and "B3LYP", respectively. Likewise, the total fractionation factor is shown for both calculation methods of ln K_{fs}. All values are shown in units of ‰ (permil). The computational methods are described above.

Reaction	Isotope pair	ln K_{fs}		ln K_{nm}	ε^{eq}	
		HF	B3LYP		HF	B3LYP
$U^{VI}O_2(CO_3)_3^{4-} \longrightarrow CaU^{IV}(PO_4)_2$	233/235	−2.03	−1.36	0.58	−1.45	−0.78
	236/235	1.47	0.97	−0.29	1.18	0.68
	238/235	3.57	2.21	−0.86	2.71	1.34
$U^{VI}O_2(CO_3)_2^{2-} \longrightarrow CaU^{IV}(PO_4)_2$	233/235	−1.83	−1.17	0.55	−1.28	−0.62
	236/235	1.31	0.83	−0.27	1.04	0.56
	238/235	3.21	1.87	−0.81	2.39	1.06

Supplementary Figures
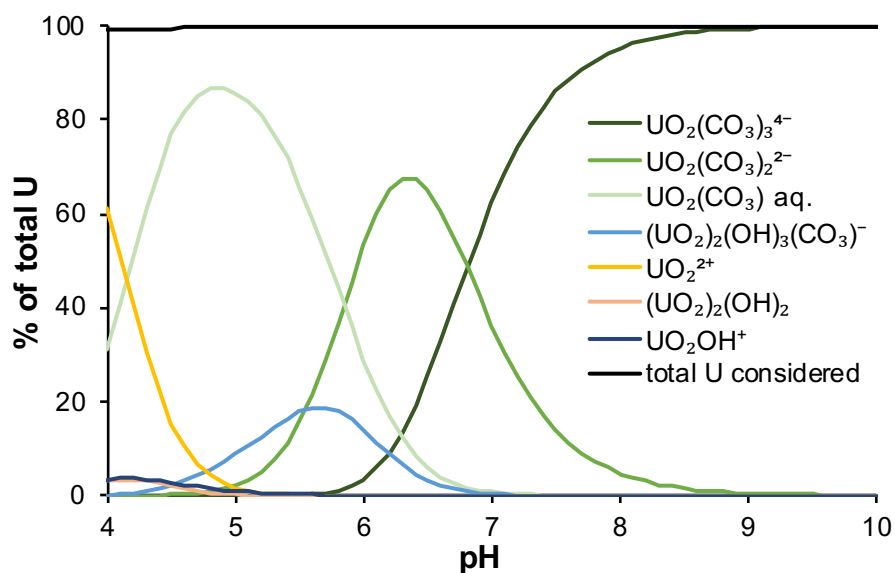
Figure S-1   Aqueous U speciation as a function of pH in systems containing 200 μM U and 30 mM sodium bicarbonate at 25 °C. Calculations were performed using MINEQL+ v5 using updated formation constants for uranium carbonate complexes (Guillaumont *et al.*, 2003; Hummel *et al.*, 2005). Below pH ~5.5, only U species contributing >0.5 % of the total U have been included in the plot in order to simplify visualisation.
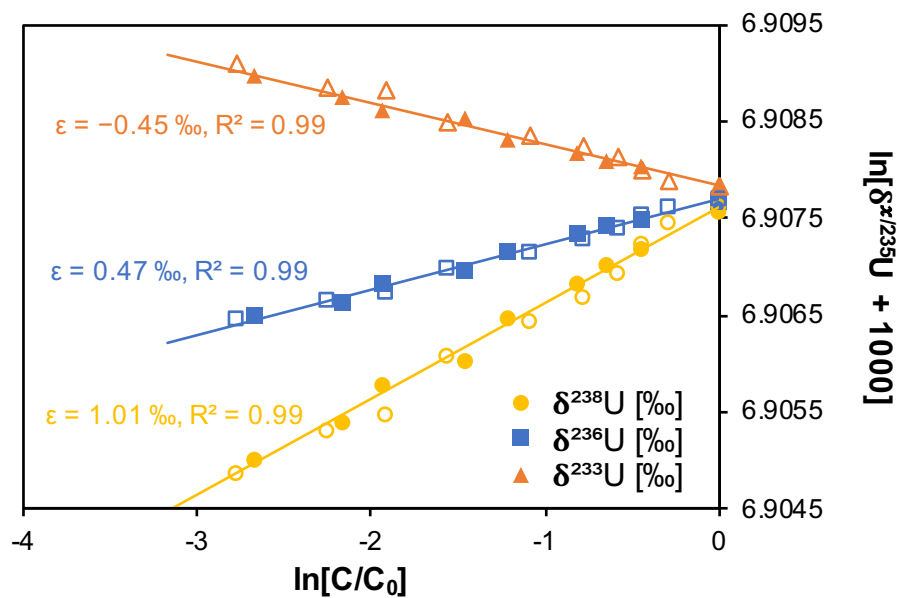
Figure S-2   Linearised plots of $\delta^{x/235}U$ isotope signatures, as a function of reaction progression. Filled and open symbols depict duplicate reactors. Linear regressions represent Rayleigh distillation models and their corresponding isotope enrichment factors (ε) and R^2 values for the mean of duplicate reactors.
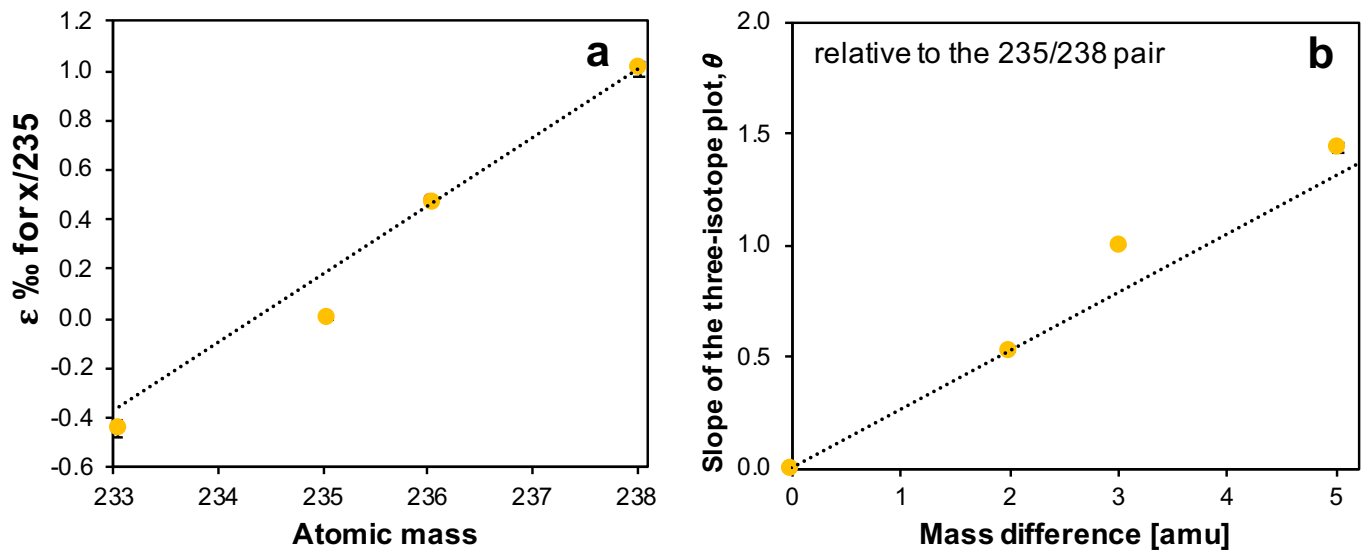
Figure S-3   **(a)** Fractionation factors (ε) for each atomic mass. Symbols and error bars depict the mean and standard deviation of duplicate reactors. Where not visible, the error is within the size of the symbol. The dotted line represents the linear regression of the even isotopes only. **(b)** Slopes of the three-isotope plots, θ, relative to the $^{235}U/^{238}U$ pair. Slopes were calculated according to Nomura *et al.* (1996) and defined as follows: $\theta = \ln \beta_{(j/238)} / \ln \beta_{(235/238)}$, where $j = 233, 235, 236$ or 238 and $\beta_{(j/238)} = r_{(j/238),i} / r_{(j/238),0}$. Here, r represents the isotopic ratio for the respective isotope pairs for a given sample (i) or the starting material (0). The mass difference of $0 = {}^{238}U$, $2 = {}^{236}U$, $3 = {}^{235}U$ and $5 = {}^{233}U$. The dotted line represents the linear regression of the even isotopes only.
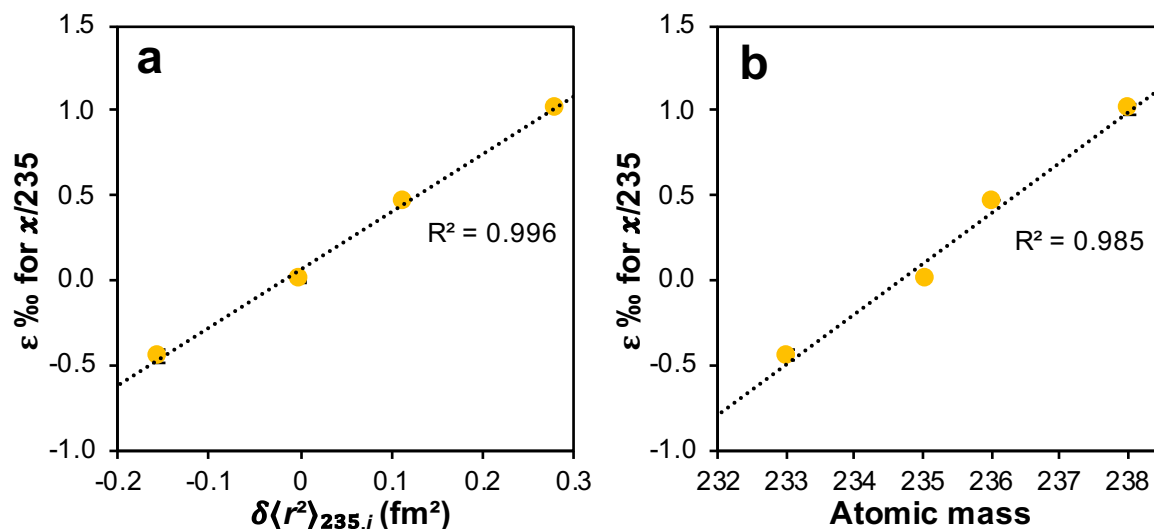
Figure S-4 **(a)** Fractionation factors (ε) for the mean square nuclear charge radii of each isotope ($\delta\langle r^2 \rangle_{235,i} = \delta\langle r^2 \rangle_i - \delta\langle r^2 \rangle_{235}$). Symbols and error bars depict the mean and standard deviation of duplicate reactors. Where not visible, the error is within the size of the symbol. Mean square nuclear charge radii for each atomic mass were taken from Angeli and Marinova (2013). **(b)** Fractionation factors (ε) for each atomic mass. Symbols and error bars depict the mean and standard deviation of duplicate reactors. Where not visible, the error is within the size of the symbol.
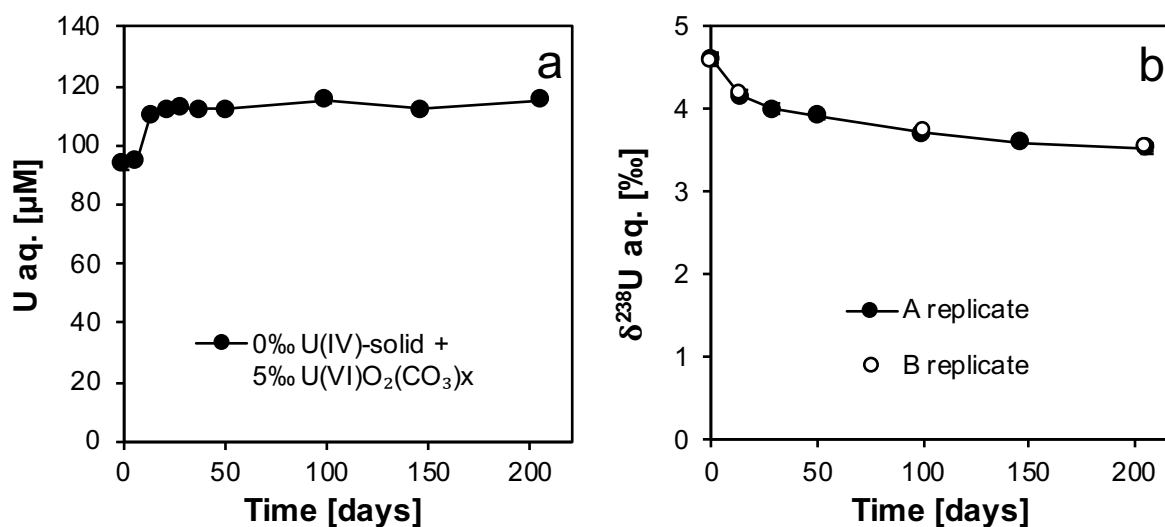
Figure S-5 **(a)** Aqueous uranium concentrations during equilibrium isotope exchange experiments between ~100 μM aqueous U^{VI}-carbonate (30 mM sodium bicarbonate) with an initial isotopic composition of ~5 ‰ and ~43 μM of solid U^{IV} product of the bioreduction experiments with an initial isotopic composition of 0 ‰. Samples were filtered through 0.22 μm filters. Symbols and error bars depict 1 standard deviation of the mean of duplicate reactors. Where not visible, the error is smaller than the symbol size. **(b)** $\delta^{238}U$ values of the aqueous U over time. Symbols and error bars depict 2 standard deviations of the mean of triplicate measurements.
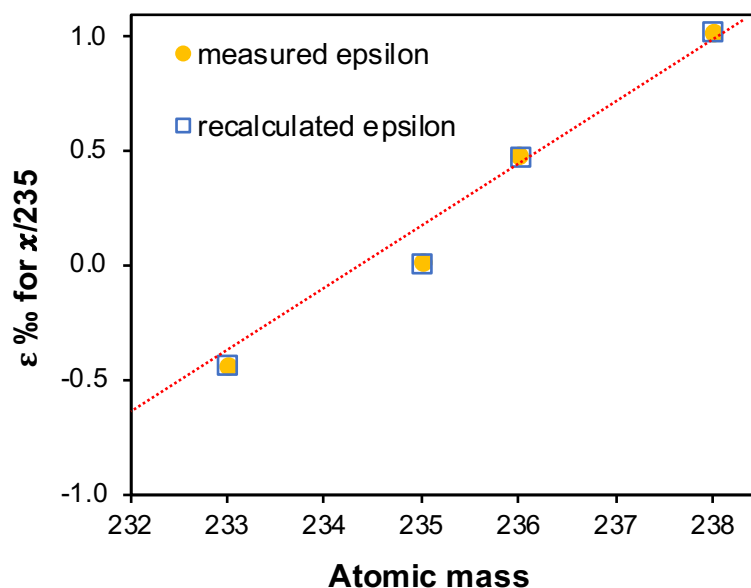
Figure S-6   Isotope enrichment factors, ε, for each atomic mass with respect to ^{235}U. Recalculated values represent the sum of the extracted mass and nuclear volume terms, determined by the methods described by Fujii *et al.* (2009) and Moynier *et al.* (2009), after Bigeleisen (1996). The dotted red line represents the linear regression of the recalculated values of the even isotopes only and indicates the presence of the odd-even staggering trend (deviation from mass dependence).

Supplementary Information References

Alessi, D.S., Lezama-Pacheco, J.S., Stubbs, J.E., Janousch, M., Bargar, J.R., Persson, P., Bernier-Latmani, R. (2014) The product of microbial uranium reduction includes multiple species with U(IV)-phosphate coordination. *Geochimica et Cosmochimica Acta* 131, 115–127. https://doi.org/10.1016/j.gca.2014.01.005

Angeli, I., Marinova, K.P. (2013) Table of experimental nuclear ground state charge radii: An update. *Atomic Data and Nuclear Data Tables* 99, 69–95. https://doi.org/10.1016/j.adt.2011.12.006

Becke, A.D. (1993) Density-functional thermochemistry. III. The role of exact exchange. *The Journal of Chemical Physics* 98, 5648–5652. https://doi.org/10.1063/1.464913

Bernier-Latmani, R., Veeramani, H., Vecchia, E.D., Junier, P., Lezama-Pacheco, J.S., Suvorova, E.I., Sharp, J.O., Wigginton, N.S., Bargar, J.R. (2010) Non-uraninite Products of Microbial U(VI) Reduction. *Environmental Science & Technology* 44, 9456–9462. https://doi.org/10.1021/es101675a

Bigeleisen, J. (1996) Nuclear Size and Shape Effects in Chemical Reactions. Isotope Chemistry of the Heavy Elements. *Journal of the American Chemical Society* 118, 3676–3680. https://doi.org/10.1021/ja954076k

Bigeleisen, J., Mayer, M.G. (1947) Calculation of Equilibrium Constants for Isotopic Exchange Reactions. *The Journal of Chemical Physics* 15, 261–267. https://doi.org/10.1063/1.1746492

Brennecka, G.A., Wasylenki, L.E., Bargar, J.R., Weyer, S., Anbar, A.D. (2011) Uranium Isotope Fractionation during Adsorption to Mn-Oxyhydroxides. *Environmental Science & Technology* 45, 1370–1375. https://doi.org/10.1021/es103061v

Cao, X., Dolg, M. (2004) Segmented contraction scheme for small-core actinide pseudopotential basis sets. *Journal of Molecular Structure: THEOCHEM* 673, 203–209. https://doi.org/10.1016/j.theochem.2003.12.015

Dyall, K.G. (2007) Relativistic double-zeta, triple-zeta, and quadruple-zeta basis sets for the actinides Ac–Lr. *Theoretical Chemistry Accounts* 117, 491–500. https://doi.org/10.1007/s00214-006-0175-4

Filatov, M. (2007) On the calculation of Mössbauer isomer shift. *The Journal of Chemical Physics* 127, 084101. https://doi.org/10.1063/1.2761879

Fricke, B., Waber, J.T. (1972) Calculation of Isomer Shift in Mössbauer Spectroscopy. *Physical Review B* 5, 3445–3449. https://doi.org/10.1103/PhysRevB.5.3445

Frisch, M.J., Trucks, G.W., Schlegel, H.B., Scuseria, G.E., Robb, M.A., *et al.* (2009) *Gaussian 09, Revision C.01*. Gaussian, Inc., Wallingford, CT. https://gaussian.com/g09_c01/

Fujii, T., Moynier, F., Albarède, F. (2009) The nuclear field shift effect in chemical exchange reactions. *Chemical Geology* 267, 139–156. https://doi.org/10.1016/j.chemgeo.2009.06.015

Guillaumont, R., Fanghänel, T., Fuger, J., Grenthe, I., Neck, V., Palmer, D.A., Rand, M.H. (2003) *Update on the Chemical Thermodynamics of Uranium, Neptunium, Plutonium, Americium and Technetium*. OECD Nuclear Energy Agency, Issy-les-Moulineaux, and Elsevier, Amsterdam.

Hummel, W., Anderegg, G., Puigdomènech, I., Rao, L., Tochiyama, O. (2005) *Chemical Thermodynamics of Compounds and Complexes of U, Np, Pu, Am, Tc, Se, Ni and Zr with Selected Organic Ligands*. OECD Nuclear Energry Agency, Issy-les-Moulineaux, and Elsevier, Amsterdam.

Iliaš, M., Saue, T. (2007) An infinite-order two-component relativistic Hamiltonian by a simple one-step transformation. *The Journal of Chemical Physics* 126, 064102. https://doi.org/10.1063/1.2436882

Jensen, H.J.A., Bast, R., Saue, T., Visscher, L., Bakken, V., *et al.* (2016) DIRAC, a relativistic *ab initio* electronic structure program, Release DIRAC16. http://www.diracprogram.org/

Knecht, S., Fux, S., van Meer, R., Visscher, L., Reiher, M., Saue, T. (2011) Mössbauer spectroscopy for heavy elements: a relativistic benchmark study of mercury. *Theoretical Chemistry Accounts* 129, 631–650. https://doi.org/10.1007/s00214-011-0911-2

Knecht, S., Repisky, M., Jensen, H.J.A., Saue, T. (2022) Exact two-component Hamiltonians for relativistic quantum chemistry: Two-electron picture-change corrections made simple. *The Journal of Chemical Physics* 157, 114106. https://doi.org/10.1063/5.0095112

Küchle, W., Dolg, M., Stoll, H., Preuss, H. (1994) Energy-adjusted pseudopotentials for the actinides. Parameter sets and test calculations for thorium and thorium monoxide. *The Journal of Chemical Physics* 100, 7535–7542. https://doi.org/10.1063/1.466847

Lee, C., Yang, W., Parr, R.G. (1988) Development of the Colle-Salvetti correlation-energy formula into a functional of the electron density. *Physical Review B* 37, 785–789. https://doi.org/10.1103/PhysRevB.37.785

Li, H., Tissot, F.L.H. (2023) UID: The uranium isotope database. *Chemical Geology* 618, 121221. https://doi.org/10.1016/j.chemgeo.2022.121221

Liu, W. (2010) Ideas of relativistic quantum chemistry. *Molecular Physics* 108, 1679–1706. https://doi.org/10.1080/00268971003781571

Moynier, F., Fujii, T., Telouk, P. (2009) Mass-independent isotopic fractionation of tin in chemical exchange reaction using a crown ether. *Analytica Chimica Acta* 632, 234–239. https://doi.org/10.1016/j.aca.2008.11.015

Nomura, M., Higuchi, N., Fujii, Y. (1996) Mass Dependence of Uranium Isotope Effects in the U(IV)−U(VI) Exchange Reaction. *Journal of the American Chemical Society* 118, 9127–9130. https://doi.org/10.1021/ja954075s

Noordmann, J., Weyer, S., Montoya-Pino, C., Dellwig, O., Neubert, N., Eckert, S., Paetzel, M., Böttcher, M.E. (2015) Uranium and molybdenum isotope systematics in modern euxinic basins: Case studies from the central Baltic Sea and the Kyllaren fjord (Norway). *Chemical Geology* 396, 182–195. https://doi.org/10.1016/j.chemgeo.2014.12.012

Richter, S., Eykens, R., Kühn, H., Aregbe, Y., Verbruggen, A., Weyer, S. (2010) New average values for the $n(^{238}U)/n(^{235}U)$ isotope ratios of natural uranium standards. *International Journal of Mass Spectrometry* 295, 94–97. https://doi.org/10.1016/j.ijms.2010.06.004

Sato, A., Bernier-Latmani, R., Hada, M., Abe, M. (2021) Ab initio and steady-state models for uranium isotope fractionation in

multi-step biotic and abiotic reduction. *Geochimica et Cosmochimica Acta* 307, 212–227. https://doi.org/10.1016/j.gca.2021.05.044

Saue, T. (2011) Relativistic Hamiltonians for Chemistry: A Primer. *ChemPhysChem* 12, 3077–3094. https://doi.org/10.1002/cphc.201100682

Saue, T., Bast, R., Gomes, A.S.P., Jensen, H.J.A., Visscher, L., *et al.* (2020) The DIRAC code for relativistic molecular calculations. *The Journal of Chemical Physics* 152, 204104. https://doi.org/10.1063/5.0004844

Scalmani, G., Frisch, M.J. (2010) Continuous surface charge polarizable continuum models of solvation. I. General formalism. *The Journal of Chemical Physics* 132, 114110. https://doi.org/10.1063/1.3359469

Scott, K.M., Lu, X., Cavanaugh, C.M., Liu, J.S. (2004) Optimal methods for estimating kinetic isotope effects from different forms of the Rayleigh distillation equation. *Geochimica et Cosmochimica Acta* 68, 433–442. https://doi.org/10.1016/S0016-7037(03)00459-9

Stephens, P.J., Devlin, F.J., Chabalowski, C.F., Frisch, M.J. (1994) Ab Initio Calculation of Vibrational Absorption and Circular Dichroism Spectra Using Density Functional Force Fields. *The Journal of Physical Chemistry* 98, 11623–11627. https://doi.org/10.1021/j100096a001

Stylo, M., Neubert, N., Wang, Y., Monga, N., Romaniello, S.J., Weyer, S., Bernier-Latmani, R. (2015) Uranium isotopes fingerprint biotic reduction. *Proceedings of the National Academy of Sciences* 112, 5619–5624. https://doi.org/10.1073/pnas.1421841112

Visscher, L., Dyall, K.G. (1997) Dirac–Fock atomic electronic structure calculations using different nuclear charge distributions. *Atomic Data and Nuclear Data Tables* 67, 207–224. https://doi.org/10.1006/adnd.1997.0751

Weyer, S., Anbar, A.D., Gerdes, A., Gordon, G.W., Algeo, T.J., Boyle, E.A. (2008) Natural fractionation of $^{238}U/^{235}U$. *Geochimica et Cosmochimica Acta* 72, 345–359. https://doi.org/10.1016/j.gca.2007.11.012

Young, E.D., Galy, A., Nagahara, H. (2002) Kinetic and equilibrium mass-dependent isotope fractionation laws in nature and their geochemical and cosmochemical significance. *Geochimica et Cosmochimica Acta* 66, 1095–1104. https://doi.org/10.1016/S0016-7037(01)00832-8

Zheng, W., Hintelmann, H. (2010) Nuclear Field Shift Effect in Isotope Fractionation of Mercury during Abiotic Reduction in the Absence of Light. *The Journal of Physical Chemistry A* 114, 4238–4245. https://doi.org/10.1021/jp910353y